Native true amplitude and phase broadband sensing now available with the latest MEMS sensors

Nicolas Tellier, Stéphane Laroche and Philippe Herrmann, Sercel*

Summary

MEMS sensors have been available for seismic applications since the early 2000s. Although the 1st generation of MEMS had a proven track record of success, in particular for 3C applications, it had some difficulty in 1C to compete in terms of cost with sparser acquisitions using arrays, and to meet the requirements of the trend towards low-frequencies due to noise performance at the lower end of the spectrum. The latest generation of MEMS, however, has overcome these limitations and indeed shows additional benefits over geophones. The digital fidelity offered by the sensor enables the recording of seismic data with true amplitude and phase and in contrast to geophones its response is unaffected by manufacturing tolerances, ageing and temperature. In addition, having power consumption and cost now lower than that of a geophone connected to an ADC, these sensors are excellent candidates to complement the industry's growing use of nodal acquisition in land surveys. For OBN applications these 3C MEMS sensors provide excellent vector fidelity with a native true vertical Z component. Two field tests, in land and OBN, were recently organized to illustrate the advantages of MEMS over geophones. The results of the two tests are herein presented and discussed.

Introduction: sensors and nodal acquisition

Trace density is now widely recognized as the key parameter to improve imaging quality and make reservoir analysis more accurate (Ourabah 2015, Michou 2017). Higher trace densities are enabled in land by aggressive productivity techniques, combined with the use of smaller receiver arrays or point receivers. The introduction of a multiplicity of land nodes to the market clearly illustrates this trend. In marine, the share of ocean-bottom nodes equipped with 3C geophones and a hydrophone continues to increase to the detriment of streamer acquisitions, and here too in combination with aggressive shooting methodologies. Another strong tendency in seismic is digitalization, but perhaps surprisingly, it has not yet greatly impacted seismic acquisition. Although a century old technology, analog sensors remain the standard, despite their inherent shortcomings that alter the fidelity of the signal recorded. Although geophones still offer a viable solution in land when deploying arrays, it may be time however to reconsider the receiver technology that best complements the industry's transition towards single sensor or nodal acquisition. In OBN, the performance of 3C MEMS sensors make them an ideal candidate to replace the shortcomings of the traditional 15 Hz omni-tilt geophones. The results of recent land and OBN field tests confirm these assertions.

About MEMS sensors

For seismic applications, MEMS sensors remain the primary alternative to geophones whose response is damped below their natural frequency and distorted above their spurious frequency. MEMS sensors also provide linear and flat amplitude and phase responses from DC to 400 Hz in the acceleration domain and their specifications are not affected by temperature, ageing or manufacturing tolerances (Figure 1). As a result the signal recorded is accurate in both phase and amplitude across the entire seismic bandwidth of interest.

	5 Hz geophone	10 Hz geophone
Natural frequency (Hz)	5 (± 7.5%)	10 (± 5%)
Sensitivity (V/m/s)	80 (± 5%)	22.7 (± 5%)
Damping	0.6 (± 7.5%)	0.6 (± 5%)

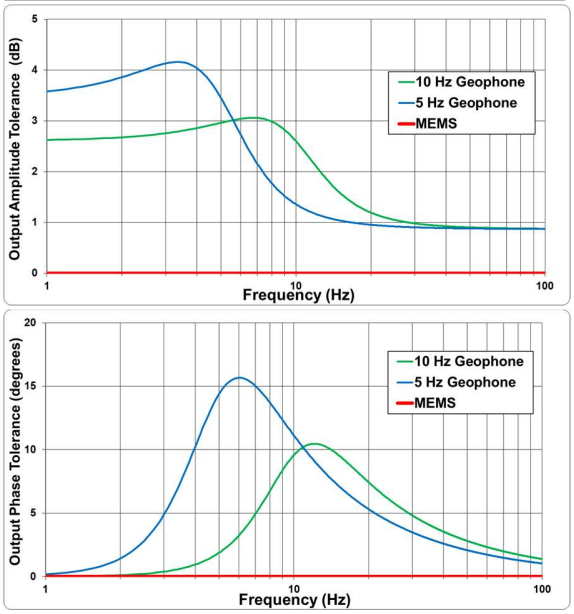

Figure 1: Illustration of sensors' manufacturing tolerances. Top: commercial 5 Hz and 10 Hz geophone specifications. The two graphs below display the maximum deviation in amplitude and phase response for these two geophones (worst case for the three specifications listed, ageing and temperature not being accounted for), compared to a MEMS.

The preservation of amplitudes has been recognized for AVO applications (Shi 2009, Lv 2013). The coil-free design makes the MEMS insensitive to electromagnetic noise, and distortion (-90 dB) is much lower than that of geophones

True amplitude and phase broadband sensing with latest MEMS sensors

(-62 dB). Since their introduction, MEMS sensors have seen use across a wide range of applications, e.g., thin gas reservoir identification (for the preservation of far offset AVO), detection of tight oil (for the phase consistency) and high-resolution shallow surveys (for the ease of deployment and preservation of high-frequency signal). By extending the fidelity of digital technology to the entire acquisition chain MEMS sensors appear to be excellent candidates to address the industry's increasing appetite for high trace density, single receiver surveys.

The previous generation of MEMS sensors (with a noise floor rated 40-45 ng/√Hz across the 10-200 Hz bandwidth, and ~120 ng/√Hz @ 1-10 Hz) suffered a significant increase in instrument noise below 3-4 Hz that compromised signal fidelity. The latest generation of MEMS (noise floor 15 ng/√Hz @ 10-200 Hz and 30 ng/√Hz @ 1-10 Hz, Lainé 2014) overcame this limitation. Indeed a single receiver has been demonstrated capable of detecting a 4,000 km distant magnitude 7 earthquake, with seismic data recorded in the 0.02-5 Hz bandwidth (Fougerat 2018).

In 3C surveys, MEMS sensors offer indisputable advantages over geophones and have long been the receiver of choice over analog tri-phones:

- From an operational perspective, the 3C MEMS assembly is omni-tilt and compact. The same basic sensor can be used for each of the three components, while geophones must be modified to compensate for gravity when operated horizontally. The MEMS tiny size allows for a correspondingly small housing, thus enabling an efficient rejection of parasitic signals, such as surface wave induced rotations. The compactness of the resulting package also favours optimal coupling to the ground – a paramount factor for the successful recording of horizontal components.
- But the major benefit of 3C MEMS lies perhaps in their excellent vector fidelity. Quality MEMS accelerometers are fitted with a feedback loop that enables the measurement of static signals (DC/0 Hz), such as Earth gravity. Thanks to this feature and contrary to that with 3C geophones, they can be easily factory-calibrated using a very accurate gravitational acceleration reference, thus compensating for the manufacturing orthogonality tolerances of the three axes. Similarly, the planting tilt can be measured automatically and compensated for in the field. As a result, 3C MEMS sensors with DC capability exhibit much better accuracy in terms of vector fidelity: the ground acceleration is measured with a very accurate separation of horizontal and vertical components, and with true amplitude and timing. The high-fidelity data recorded in this way thus enables rigorous analysis of anisotropy.

Land and OBN field tests were organized in 2019 in order to perform a thorough sensor-to-sensor comparison and illustrate several of the benefits described hereinabove. These comparisons are to be considered as "brute", i.e., they are performed in m/s units with only a deterministic compensation for sensors response, without any hypothesis or parametrization related to seismic processing.

Land experience

Four lines of 100 receivers each were deployed in parallel with a 5 m station spacing. Four sensors were then collocated at each station: a 10 Hz geophone (SG-10), a 5 Hz high-sensitivity geophone and two low-noise MEMS, one of the MEMS integrated in a cabled system (DSU-508XT), the other one in a wireless node (WiNG DFU). As the overall results and analyses turned out to be very similar for the two low-noise MEMS systems, only data from the node system are displayed hereinbelow. A 200 VP cross-spread line was shot with a single super-heavy vibrator (Nomad 90), using a 1.5-150 Hz sweep and a low-frequency distortion reduction solution (Ollivrin, 2019) integrated in a VE464 control electronics. The distance between VPs was 2.5 m. The processing applied to the Common Receiver Gather (CRG) and time slices presented below (both in true amplitudes) was limited; for geophones, to the sensor phase and sensitivity de-signature, and for the MEMS, to the integration of the acceleration data into velocity.

Sensors' low-frequency capability

An example CRG is presented in figure 2 for three collocated sensors, with the full CRG bandwidth and its spectral decomposition in four low-frequency octaves. These CRGs provide a necessarily raw but compelling demonstration of the sensors' ability to recover low-frequency signal, with the MEMS outperforming the 5 Hz geophone, that itself outperforms the 10 Hz geophone. The differences are particularly marked on the lower frequency panels, and lessen as frequencies increase. Differences can hardly be seen on higher frequency panels (16-32 Hz and above, not displayed). At a time when low-frequency signal recovery becomes a must-have for imaging these results provide two facts that merit consideration:

- Despite the relatively recent introduction of 5 Hz geophones, 10 Hz geophones still remain the industry benchmark. There are nonetheless clear benefits in the transition towards sensors capable of recording low frequencies. These advantages exceed those provided by hydraulic vibrators excessively boosted for the low frequencies (Tellier 2019).
- The limitations of MEMS sensors at low frequencies have been overcome with the latest generation (Lainé 2014), though it somehow takes time for the industry to acknowledge it (Monk 2020).

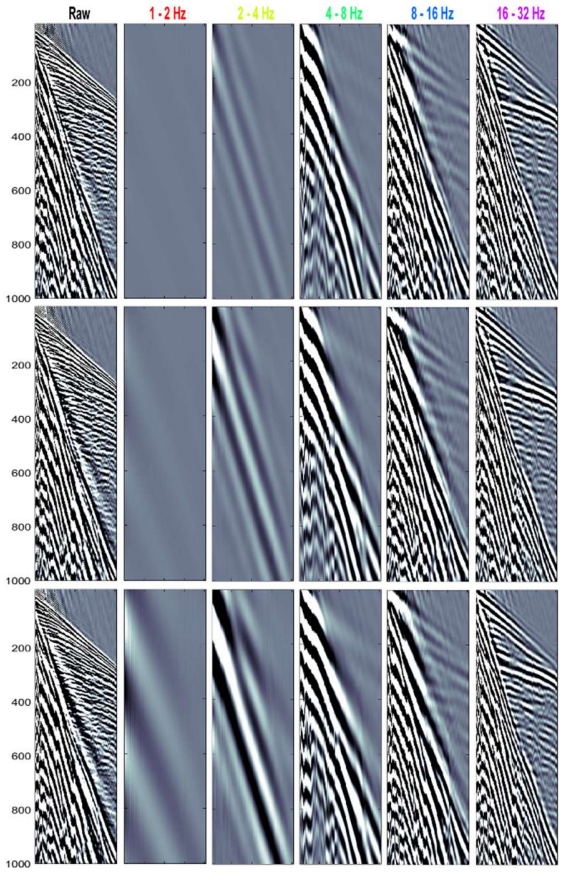

Figure 2: CRG gathers with full signal bandwidth (left) and frequency panels for the first four octaves (right): 10 Hz geophone (top), 5 Hz geophone (middle) and MEMS (bottom).

Sensors' manufacturing tolerances at low frequencies

Times slices at 350 ms are presented in figure 3, with a 2-4 Hz bandpass filter. As all the source points and receivers contributed to these displays, they provide a good statistical synthesis of the sensor capability with regard to the data acquired during the test. Note that the 10 Hz geophone is not displayed, due to both lack of available space and results that were greatly inferior to the other two sensors. Two main differences can be seen. Firstly, the wave front delineation is much sharper on the MEMS data. Secondly, stripes visible on the geophone data are not evident on the MEMS data. As special care was observed when planting/coupling the sensors, this effect can only be related to the variation in response between individual geophones. This effect could be observed up to the 4-8 Hz panel for 5 Hz geophones, and 8-16 Hz panel for the 10 Hz geophones. It corresponds to the low-frequency bandwidth where the geophone manufacturing tolerances are most pronounced (i.e. the influence, besides sensitivity, of the natural frequency and damping), and where the single de-signature operator commonly used cannot compensate for these sensor-to-sensor variations.

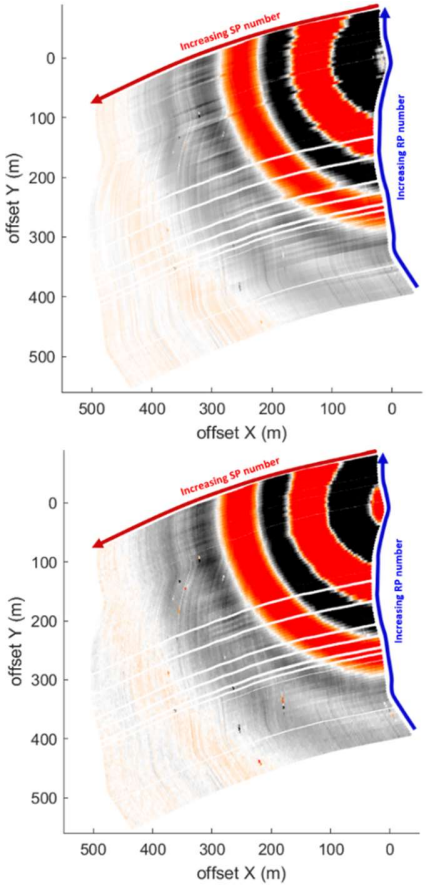

Figure 3: Time slices at 350 ms for 5 Hz geophones (top) and MEMS (bottom), with 2-4 Hz bandpass filter. White curves correspond to receiver locations skipped due to obstacles.

OBN experience

It is worth noting that MEMS sensors already enjoy a proven track record of success in ocean-bottom cable systems (e.g., SeaRay system, see Archer 2012 and Keggin 2017). However a 3C MEMS sensor equipped OBN system has been introduced very recently and a comparative field test carried out. Two lines of 28 ocean-bottom nodes were deployed at shallow depth (20-30 m). At each receiver station (spaced 100 m), two nodes were collocated, one equipped with standard 15 Hz 3C geophones, the other with low-noise 3C MEMS. A 10 km source line was shot with a 25 m source interval. The source available for the test was regrettably not designed for low frequencies, somewhat limiting the scope of analyses.

True amplitude and phase broadband sensing with latest MEMS sensors

The analysis of this test campaign is still ongoing at the time of redacting this abstract, however, several characteristics of the MEMS data are already clearly superior to that of the geophone data. The processing applied for the sensor CRGs presented below (both in true amplitudes) was limited to sensor de-signature (for geophones: phase and amplitude compensation for natural frequency, damping and sensitivity; for MEMS: integration from acceleration to velocity and sensitivity compensation). The vertical component (Z) was reconstructed by using the tilt sensor measurement for geophones, and the built-in sensor tilt determination for MEMS.

Sensors' high-frequency capability

Figure 4 shows a sample of Z CRG after the application of a 100-200 Hz bandpass filter. As with the other 27 CRGs analysed, the geophone CRG shows a significant high-frequency contamination, in the form of "drips" following the recording of the energetic, high-frequency water layer direct arrival. This contamination was not observed on the MEMS and hydrophone data, nor on the X, Y geophone components. At this stage, no sound explanation has been found for this observation.

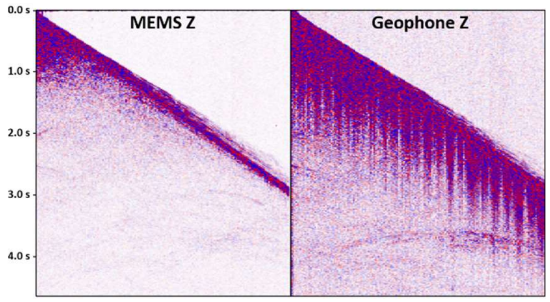

Figure 4: Example of Z CRG in m/s (100-200 Hz bandwidth) for MEMS (left) and geophone (right) vertical components.

Verticality

Figure 5 displays a sample of a Z CRG after the application of a 16-31 Hz bandpass filter. While the MEMS Z data is seen to contain only vertical signal, the data recorded by its geophone counterpart also contains non-vertical signal. The difference between the two sensors (that which does not contain reflected PP waves, and thus illustrates the performance of the sensor de-signature) confirms this observation: it is dominated by water layer direct arrivals and vertically propagating PS waves. These two waves, polarized perpendicularly to the vertical, demonstrate a difference of verticality between the two sensors. A detailed study of the direct water layer arrival showed an exact verticality of the MEMS, but an erroneous one for the geophones. This verticality error, observed on all 28 geophone CRGs, indicates that it is not related to an isolated failure of a tilt sensor on a given geophone node; it cannot in addition be corrected by processing means, due to strong interference between the different wave types in a shallow water context. This interference would also predominate in records acquired with blended acquisition, now a standard acquisition technique in OBN. This non-verticality of geophones can also be observed in figure 4, with the presence of high-frequency diffractions at unexpected times ($t > 3$ s). Unlike 3C geophones, MEMS 3C sensors thus enable direct access to built-in true verticality.

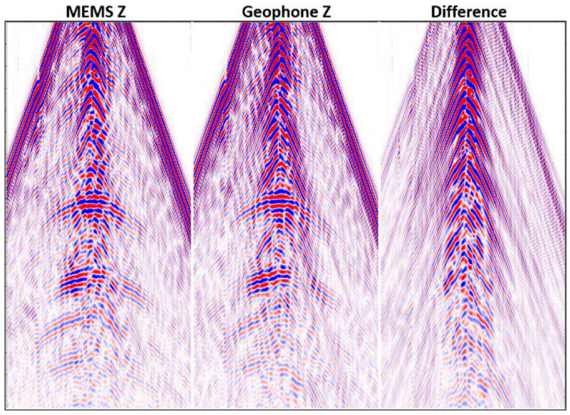

Figure 5: Example of CRG in m/s, 16-31 Hz bandpass filter, time window 0.5-2.2 s.

As a final remark, the impact of the variations in geophone specifications on seismic data discussed earlier could also be observed on this dataset below 16 Hz (not illustrated).

Conclusions and discussions

Two recent field tests provided confirmation of multiple benefits of MEMS sensors over geophones, in particular their superior broadband capability (both in low and high frequencies), their excellent verticality when used as 3C sensors, and the fidelity of their recorded signal as it is not subject to performance variations within the range of sensor tolerances. The analysis of the datasets acquired is at the time of writing continuing, further results will be presented and discussed.

Acknowledgments

The authors would like to thank Smart Seismic Solutions and BGP Offshore (in particular, Liu Haibo and Xu Zhaohong) for their support in field test organization, Didier Marin (CGG) for its valuable support and expertise in data processing, and their numerous Sercel colleagues who contributed to the success of the test acquisition campaign and analysis.

References

Archer, J., L. Bell, M. Hall, G. Margrave, K. Hall, and M. Bertram, 2012, Obtaining low frequency seismic data, onshore and in shallow water: First Break Vol 30, No.1, pp. 79-87. DOI: https://doi.org/0.3997/1365-2397.30.1.56179

Fougerat, A., L. Guérineau, and N. Tellier, 2018, High-quality signal recording down to 0.001 Hz with standard MEMS accelerometers: SEG 88th Annual Meeting, expanded abstract. DOI: https://doi.org/10.1190/segam2018-2995544.1

Keggin, J., W. Alaaraji, and J. Zhou, 2017, Improved images of fractured basement in Vietnam: GeoExpro, **Vol 14, No.4**, 22-25.

Lainé, J., and D. Mougenot, 2014, A high-sensitivity MEMS-based accelerometer: The Leading Edge **Vol 33 No. 11**, pp. 1234-1242. DOI: https://doi.org/10.1190/tle33111234.1

Lv S., and D. Mougenot, 2013, Do digital accelerometers preserve amplitude better? A case study: Geohorizons, **Vol.18 No.2**, July 2013.

Michou, L., L. Michel, P. Herrmann, T. Coléou, P. Feugère, and J. Formento, 2017, Survey Design Comparison Regarding Seismic Reservoir Characterization Objectives – A case study from South Tunisia. 79th EAGE conference and exhibition, extended abstract. DOI: https://doi.org/10.3997/2214-4609.201701243

Monk, D., 2020, Survey Design and Seismic Acquisition for Land, Marine, and In-between in Light of New Technology and Techniques: SEG Distinguished Instructor Short Course, chapter 1 p.18, Distinguished Instructor Series, No. 23. DOI: https://doi.org/10.1190/1.9781560803713.ch1

Ollivrin, G., and N. Tellier, 2019, SmartLF for robust and straightforward reduction of low-frequency distortion: SEG 89th Annual Meeting, expanded abstract. DOI: https://doi.org/10.1190/segam2019-3214978.1

Ourabah, A., J. Bradley, T. Hance, M. Kowalczyk-Kedzierska, M. Grimshaw, and E. Murray, 2015, Impact of Acquisition Geometry on AVO/AVOA Attributes Quality - A Decimation Study Onshore Jordan. 77th EAGE conference and exhibition, extended abstract. DOI: https://doi.org/10.3997/2214-4609.201413301

Shi, S., Y. Du, M. Zhang, S. Cheng, L. Gan et al. [2009] Seismic acquisition with digital point receivers and prestack reservoir characterization of China's Sulige gas field. The Leading Edge, 28, 324-331. DOI: https://doi.org/10.1190/1.3104079

Tellier N., and J. Lainé,, 2017, Understanding MEMS-based digital seismic sensors: First Break, **Vol 35, No.1**, pp. 93-100. DOI: https://doi.org/0.3997/1365-2397.35.1.87386

Tellier, N. and G. Ollivrin, 2019, Low-frequency Vibroseis: current achievements and the road ahead? First Break **Vol 37, No.1**, pp. 49-54. DOI: https://doi.org/10.3997/1365-2397.n0011